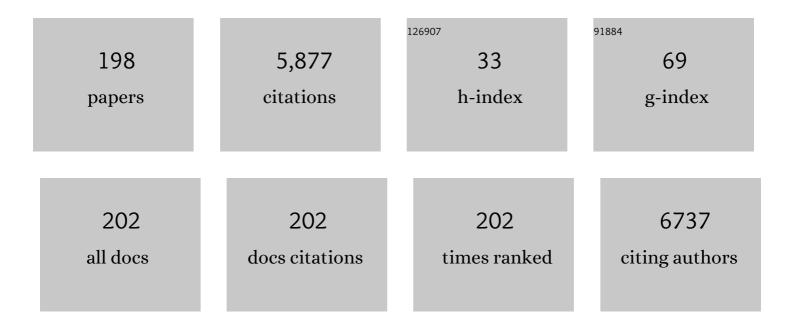
Steven Staelens

List of Publications by Year in descending order

Source: https://exaly.com/author-pdf/8796826/publications.pdf Version: 2024-02-01



#	Article	IF	CITATIONS
1	GATE: a simulation toolkit for PET and SPECT. Physics in Medicine and Biology, 2004, 49, 4543-4561.	3.0	1,765
2	U-SPECT-II: An Ultra-High-Resolution Device for Molecular Small-Animal Imaging. Journal of Nuclear Medicine, 2009, 50, 599-605.	5.0	265
3	A20 (TNFAIP3) deficiency in myeloid cells triggers erosive polyarthritis resembling rheumatoid arthritis. Nature Genetics, 2011, 43, 908-912.	21.4	250
4	Ictalâ€onset localization through connectivity analysis of intracranial <scp>EEG</scp> signals in patients with refractory epilepsy. Epilepsia, 2013, 54, 1409-1418.	5.1	116
5	Association of short-term cognitive decline and MCI-to-AD dementia conversion with CSF, MRI, amyloid- and 18F-FDG-PET imaging. NeuroImage: Clinical, 2019, 22, 101771.	2.7	108
6	Monte Carlo simulations of a scintillation camera using GATE: validation and application modelling. Physics in Medicine and Biology, 2003, 48, 3021-3042.	3.0	103
7	Influence of Skull Modeling Approaches on EEG Source Localization. Brain Topography, 2014, 27, 95-111.	1.8	88
8	The Cerebrospinal Fluid Aβ1–42/Aβ1–40 Ratio Improves Concordance with Amyloid-PET for Diagnosing Alzheimer's Disease in a Clinical Setting. Journal of Alzheimer's Disease, 2017, 60, 561-576.	2.6	82
9	Monte Carlo simulation in PET and SPECT instrumentation using GATE. Nuclear Instruments and Methods in Physics Research, Section A: Accelerators, Spectrometers, Detectors and Associated Equipment, 2004, 527, 180-189.	1.6	80
10	Validation of the GATE Monte Carlo simulation platform for modelling a CsI(Tl) scintillation camera dedicated to small-animal imaging. Physics in Medicine and Biology, 2004, 49, 271-285.	3.0	79
11	μPET imaging of the pharmacokinetic behavior of medium and high molar mass 89 Zr-labeled poly(2-ethyl-2-oxazoline) in comparison to poly(ethylene glycol). Journal of Controlled Release, 2016, 235, 63-71.	9.9	76
12	Accurate epileptogenic focus localization through time-variant functional connectivity analysis of intracranial electroencephalographic signals. NeuroImage, 2011, 56, 1122-1133.	4.2	75
13	Brain inflammation in a chronic epilepsy model: Evolving pattern of the translocator protein during epileptogenesis. Neurobiology of Disease, 2015, 82, 526-539.	4.4	69
14	Performance evaluation of small-animal multipinhole μSPECT scanners for mouse imaging. European Journal of Nuclear Medicine and Molecular Imaging, 2013, 40, 744-758.	6.4	68
15	Iterative CT Reconstruction Using Shearlet-Based Regularization. IEEE Transactions on Nuclear Science, 2013, 60, 3305-3317.	2.0	55
16	Comparison of Image Quality of Different Iodine Isotopes (I-123, I-124, and I-131). Cancer Biotherapy and Radiopharmaceuticals, 2007, 22, 423-430.	1.0	49
17	¹⁸ F-PBR111 PET Imaging in Healthy Controls and Schizophrenia: Test–Retest Reproducibility and Quantification of Neuroinflammation. Journal of Nuclear Medicine, 2018, 59, 1267-1274.	5.0	47
18	Hybrid scatter correction applied to quantitative holmium-166 SPECT. Physics in Medicine and Biology, 2006, 51, 4773-4787.	3.0	44

#	Article	IF	CITATIONS
19	Imaging brain inflammation in epilepsy. Neuroscience, 2014, 279, 238-252.	2.3	44
20	Use of the GATE Monte Carlo package for dosimetry applications. Nuclear Instruments and Methods in Physics Research, Section A: Accelerators, Spectrometers, Detectors and Associated Equipment, 2006, 569, 335-340.	1.6	43
21	An Integrated Framework to Quantitatively Link Mouse-Specific Hemodynamics to Aneurysm Formation in Angiotensin II-infused ApoE â~'/â~' mice. Annals of Biomedical Engineering, 2011, 39, 2430-2444.	2.5	43
22	Characterization of [99mTc]Duramycin as a SPECT Imaging Agent for Early Assessment of Tumor Apoptosis. Molecular Imaging and Biology, 2015, 17, 838-847.	2.6	43
23	99mTc-(CO)3 His-Annexin A5 Micro-SPECT Demonstrates Increased Cell Death by Irinotecan During the Vascular Normalization Window Caused by Bevacizumab. Journal of Nuclear Medicine, 2011, 52, 1786-1794.	5.0	41
24	Replacing Vascular Corrosion Casting by In Vivo Micro-CT Imaging for Building 3D Cardiovascular Models in Mice. Molecular Imaging and Biology, 2011, 13, 78-86.	2.6	40
25	Development of a novel antibody–tetrazine conjugate for bioorthogonal pretargeting. Organic and Biomolecular Chemistry, 2016, 14, 7544-7551.	2.8	38
26	^{99m} Tc-Duramycin SPECT Imaging of Early Tumor Response to Targeted Therapy: A Comparison with ¹⁸ F-FDG PET. Journal of Nuclear Medicine, 2017, 58, 665-670.	5.0	38
27	Fast and memoryâ€efficient Monte Carloâ€based image reconstruction for wholeâ€body PET. Medical Physics, 2010, 37, 3667-3676.	3.0	37
28	Hippocampal deep brain stimulation induces decreased rCBF in the hippocampal formation of the rat. Neurolmage, 2010, 52, 55-61.	4.2	37
29	Towards a reproducible protocol for repetitive and semi-quantitative rat brain imaging with 18 F-FDG: Exemplified in a memantine pharmacological challenge. NeuroImage, 2014, 96, 276-287.	4.2	37
30	Kinetics of angiogenic changes in a new mouse model for hepatocellular carcinoma. Molecular Cancer, 2010, 9, 219.	19.2	36
31	Acceleration of GATE SPECT simulations. Medical Physics, 2008, 35, 1476-1485.	3.0	35
32	Performance Characterization of an Actively Cooled Repetitive Transcranial Magnetic Stimulation Coil for the Rat. Neuromodulation, 2016, 19, 459-468.	0.8	35
33	State-associated changes in longitudinal [18F]-PBR111 TSPO PET imaging of psychosis patients: Evidence for the accelerated ageing hypothesis?. Brain, Behavior, and Immunity, 2019, 77, 46-54.	4.1	35
34	Evaluation of 3D Monte Carlo-Based Scatter Correction for 201Tl Cardiac Perfusion SPECT. Journal of Nuclear Medicine, 2007, 48, 637-644.	5.0	34
35	<i>N</i> -Acetylcysteine– and MK-801–Induced Changes in Glutamate Levels Do Not Affect In Vivo Binding of Metabotropic Glutamate 5 Receptor Radioligand ¹¹ C-ABP688 in Rat Brain. Journal of Nuclear Medicine, 2013, 54, 1954-1961.	5.0	34
36	¹⁸ Fâ€FDG PET, the early phases and the delivery rate of ¹⁸ Fâ€AV45 PET as proxies of cerebral blood flow in Alzheimer's disease: Validation against ¹⁵ Oâ€H ₂ O PET. Alzheimer's and Dementia, 2019, 15, 1172-1182.	0.8	33

#	Article	IF	CITATIONS
37	A three-dimensional theoretical model incorporating spatial detection uncertainty in continuous detector PET. Physics in Medicine and Biology, 2004, 49, 2337-2350.	3.0	32
38	The Label Matters: μPET Imaging of the Biodistribution of Low Molar Mass 89Zr and 18F-Labeled Poly(2-ethyl-2-oxazoline). Biomacromolecules, 2017, 18, 96-102.	5.4	32
39	Neuroimaging of Subacute Brain Inflammation and Microstructural Changes Predicts Long-Term Functional Outcome after Experimental Traumatic Brain Injury. Journal of Neurotrauma, 2019, 36, 768-788.	3.4	32
40	Validation and noninvasive kinetic modeling of [¹¹ C]UCB-J PET imaging in mice. Journal of Cerebral Blood Flow and Metabolism, 2020, 40, 1351-1362.	4.3	32
41	Reconstruction of 2D PET data with Monte Carlo generated system matrix for generalized natural pixels. Physics in Medicine and Biology, 2006, 51, 3105-3125.	3.0	31
42	In vivo evaluation of 18F-labeled TCO for pre-targeted PET imaging in the brain. Nuclear Medicine and Biology, 2014, 41, 513-523.	0.6	31
43	Early Prediction of Tumor Response to Treatment: Preclinical Validation of ^{99m} Tc-Duramycin. Journal of Nuclear Medicine, 2016, 57, 805-811.	5.0	30
44	Non-invasive PET imaging of brain inflammation at disease onset predicts spontaneous recurrent seizures and reflects comorbidities. Brain, Behavior, and Immunity, 2017, 61, 69-79.	4.1	30
45	Accurate Monte Carlo modelling of the back compartments of SPECT cameras. Physics in Medicine and Biology, 2011, 56, 87-104.	3.0	29
46	Validation of the Semiquantitative Static SUVR Method for ¹⁸ F-AV45 PET by Pharmacokinetic Modeling with an Arterial Input Function. Journal of Nuclear Medicine, 2017, 58, 1483-1489.	5.0	29
47	In vivo molecular neuroimaging of glucose utilization and its association with fibrillar amyloid-l² load in aged APPPS1-21 mice. Alzheimer's Research and Therapy, 2015, 7, 76.	6.2	27
48	Longitudinal quantification of inflammation in the murine dextran sodium sulfate-induced colitis model using μPET/CT1. Inflammatory Bowel Diseases, 2011, 17, 2058-2064.	1.9	26
49	Noninvasive Relative Quantification of [11C]ABP688 PET Imaging in Mice Versus an Input Function Measured Over an Arteriovenous Shunt. Frontiers in Neurology, 2018, 9, 516.	2.4	26
50	Fast hybrid SPECT simulation including efficient septal penetration modelling (SP-PSF). Physics in Medicine and Biology, 2007, 52, 3027-3043.	3.0	24
51	Resting-state functional MRI and [18F]-FDG PET demonstrate differences in neuronal activity between commonly used mouse strains. NeuroImage, 2016, 125, 571-577.	4.2	24
52	Evaluation of Small-Animal PET Outcome Measures to Detect Disease Modification Induced by BACE Inhibition in a Transgenic Mouse Model of Alzheimer Disease. Journal of Nuclear Medicine, 2017, 58, 1977-1983.	5.0	24
53	Dipole estimation errors due to not incorporating anisotropic conductivities in realistic head models for EEG source analysis. Physics in Medicine and Biology, 2009, 54, 6079-6093.	3.0	23
54	Fast simulation of yttriumâ€90 bremsstrahlung photons with <scp>GATE</scp> . Medical Physics, 2010, 37, 2943-2950.	3.0	23

#	Article	IF	CITATIONS
55	Synthesis and Evaluation of a Zr-89-Labeled Monoclonal Antibody for Immuno-PET Imaging of Amyloid-β Deposition in the Brain. Molecular Imaging and Biology, 2016, 18, 598-605.	2.6	23
56	Awake ¹⁸ F-FDG PET Imaging of Memantine-Induced Brain Activation and Test–Retest in Freely Running Mice. Journal of Nuclear Medicine, 2019, 60, 844-850.	5.0	23
57	Single-Photon Emission Computed Tomographic Imaging of the Early Time Course of Therapy-Induced Cell Death Using Technetium 99m Tricarbonyl His-Annexin A5 in a Colorectal Cancer Xenograft Model. Molecular Imaging, 2012, 11, 7290.2011.00034.	1.4	22
58	The Effects of Physiological and Methodological Determinants on ¹⁸ F-FDG Mouse Brain Imaging Exemplified in a Double Transgenic Alzheimer Model. Molecular Imaging, 2016, 15, 153601211562491.	1.4	21
59	Comparing planar image quality of rotating slat and parallel hole collimation: influence of system modeling. Physics in Medicine and Biology, 2008, 53, 1989-2002.	3.0	20
60	Influence of skull conductivity perturbations on EEG dipole source analysis. Medical Physics, 2010, 37, 4475-4484.	3.0	20
61	Fast and Accurate Rat Head Motion Tracking With Point Sources for Awake Brain PET. IEEE Transactions on Medical Imaging, 2017, 36, 1573-1582.	8.9	20
62	¹⁸ F-Flortanidazole Hypoxia PET Holds Promise as a Prognostic and Predictive Imaging Biomarker in a Lung Cancer Xenograft Model Treated with Metformin and Radiotherapy. Journal of Nuclear Medicine, 2019, 60, 34-40.	5.0	20
63	In vitro and in vivo evaluation of [99mTc]-labeled tricarbonyl His-annexin A5 as an imaging agent for the detection of phosphatidylserine-expressing cells. Nuclear Medicine and Biology, 2010, 37, 965-975.	0.6	19
64	Small-animal repetitive transcranial magnetic stimulation combined with [18F]-FDG microPET to quantify the neuromodulation effect in the rat brain. Neuroscience, 2014, 275, 436-443.	2.3	19
65	Accelerated high-frequency repetitive transcranial magnetic stimulation enhances motor activity in rats. Neuroscience, 2017, 347, 103-110.	2.3	19
66	PET imaging of freely moving interacting rats. NeuroImage, 2019, 191, 560-567.	4.2	19
67	An investigation of temporal regularization techniques for dynamic PET reconstructions using temporal splines. Medical Physics, 2007, 34, 1766-1778.	3.0	18
68	Cluster computing software for <scp>GATE</scp> simulations. Medical Physics, 2007, 34, 1926-1933.	3.0	18
69	Noninvasive Whole-Body Imaging of Phosphatidylethanolamine as a Cell Death Marker Using ^{99m} Tc-Duramycin During TNF-Induced SIRS. Journal of Nuclear Medicine, 2018, 59, 1140-1145.	5.0	18
70	Longitudinal Characterization of mGluR5 Using ¹¹ C-ABP688 PET Imaging in the Q175 Mouse Model of Huntington Disease. Journal of Nuclear Medicine, 2018, 59, 1722-1727.	5.0	18
71	Synaptic Vesicle Glycoprotein 2A Is Affected in the Central Nervous System of Mice with Huntington Disease and in the Brain of a Human with Huntington Disease Postmortem. Journal of Nuclear Medicine, 2022, 63, 942-947.	5.0	18
72	Development of a ligand for in vivo imaging of mutant huntingtin in Huntington's disease. Science Translational Medicine, 2022, 14, eabm3682.	12.4	18

#	Article	IF	CITATIONS
73	System characteristics of SPECT with a slat collimated strip detector. Physics in Medicine and Biology, 2006, 51, 391-405.	3.0	17
74	Reconstruction for Gated Dynamic Cardiac PET Imaging Using a Tensor Product Spline Basis. IEEE Transactions on Nuclear Science, 2007, 54, 80-91.	2.0	17
75	MR-based spatial normalization improves [18F]MNI-659 PET regional quantification and detectability of disease effect in the Q175 mouse model of Huntington's disease. PLoS ONE, 2018, 13, e0206613.	2.5	17
76	Caspase-3 probes for PET imaging of apoptotic tumor response to anticancer therapy. Organic and Biomolecular Chemistry, 2019, 17, 4801-4824.	2.8	17
77	GATE simulations for optimization of pinhole imaging. Nuclear Instruments and Methods in Physics Research, Section A: Accelerators, Spectrometers, Detectors and Associated Equipment, 2006, 569, 359-363.	1.6	16
78	Physics process level discrimination of detections for <scp>GATE</scp> : Assessment of contamination in SPECT and spurious activity in PET. Medical Physics, 2009, 36, 1053-1060.	3.0	16
79	Effect of the static magnetic field of the MR-scanner on ERPs: Evaluation of visual, cognitive and motor potentials. Clinical Neurophysiology, 2010, 121, 672-685.	1.5	16
80	Synthesis and in vivo preclinical evaluation of an 18F labeled uPA inhibitor as a potential PET imaging agent. Nuclear Medicine and Biology, 2014, 41, 477-487.	0.6	16
81	Evaluation of [18F]CP18 as a Substrate-Based Apoptosis Imaging Agent for the Assessment of Early Treatment Response in Oncology. Molecular Imaging and Biology, 2017, 19, 560-569.	2.6	16
82	Improved stability of a novel fluorine-18 labeled TCO analogue for pretargeted PET imaging. Nuclear Medicine and Biology, 2019, 76-77, 36-42.	0.6	16
83	Single-photon emission computed tomographic imaging of the early time course of therapy-induced cell death using technetium 99m tricarbonyl His-annexin A5 in a colorectal cancer xenograft model. Molecular Imaging, 2012, 11, 135-47.	1.4	16
84	SPECT imaging of high energy isotopes and isotopes with high energy contaminants with rotating slat collimators. Medical Physics, 2009, 36, 4257-4267.	3.0	15
85	Colonoscopy and µPET/CT are Valid Techniques to Monitor Inflammation in the Adoptive Transfer Colitis Model in Mice. Inflammatory Bowel Diseases, 2013, 19, 967-976.	1.9	15
86	Longitudinal Characterization of [18F]-FDG and [18F]-AV45 Uptake in the Double Transgenic TASTPM Mouse Model. Journal of Alzheimer's Disease, 2016, 55, 1537-1548.	2.6	15
87	Preclinical molecular imaging of glutamatergic and dopaminergic neuroreceptor kinetics in obsessive compulsive disorder. Progress in Neuro-Psychopharmacology and Biological Psychiatry, 2017, 77, 90-98.	4.8	15
88	In vitro and In vivo Assessment of Suitable Reference Region and Kinetic Modelling for the mGluR1 Radioligand [11C]ITDM in Mice. Molecular Imaging and Biology, 2020, 22, 854-863.	2.6	15
89	Validation of a spatially variant resolution model for small animal brain PET studies. Biomedical Physics and Engineering Express, 2020, 6, 045001.	1.2	15
90	Evolution of the GATE project: new results and developments. Nuclear Physics, Section B, Proceedings Supplements, 2007, 172, 101-103.	0.4	14

#	Article	IF	CITATIONS
91	Quantifying the Effect of Repetitive Transcranial Magnetic Stimulation in the Rat Brain by μSPECT CBF Scans. Brain Stimulation, 2013, 6, 554-562.	1.6	14
92	A simulation study on the impact of the blood flow-dependent component in [18F]AV45 SUVR in Alzheimer's disease. PLoS ONE, 2017, 12, e0189155.	2.5	14
93	Quantitative μPET Imaging of Cerebral Glucose Metabolism and Amyloidosis in the TASTPM Double Transgenic Mouse Model of Alzheimer's Disease. Current Alzheimer Research, 2015, 12, 694-703.	1.4	14
94	Preclinical Evaluation of Monoclonal Antibody 14C5 for Targeting Pancreatic Cancer. Cancer Biotherapy and Radiopharmaceuticals, 2010, 25, 193-205.	1.0	13
95	Radiosynthesis and in vivo evaluation of [11C]-labelled pyrrole-2-carboxamide derivates as novel radioligands for PET imaging of monoamine oxidase A. Nuclear Medicine and Biology, 2010, 37, 459-467.	0.6	13
96	Antitumour Efficacy of Two Paclitaxel Formulations for Hyperthermic Intraperitoneal Chemotherapy (HIPEC) in an In Vivo Rat Model. Pharmaceutical Research, 2011, 28, 1653-1660.	3.5	13
97	Rat Brain Normalization Templates for Robust Regional Analysis of [11 C]ABP688 Positron Emission Tomography/Computed Tomography. Molecular Imaging, 2015, 14, 7290.2014.00037.	1.4	13
98	Efficacy Screening of <i>Gloriosa Superba</i> Extracts in a Murine Pancreatic Cancer Model Using ¹⁸ F-FDG PET/CT for Monitoring Treatment Response. Cancer Biotherapy and Radiopharmaceuticals, 2016, 31, 99-109.	1.0	13
99	Multiprobe molecular imaging of an NMDA receptor hypofunction rat model for glutamatergic dysfunction. Psychiatry Research - Neuroimaging, 2016, 248, 1-11.	1.8	13
100	The effect of occipital nerve field stimulation on the descending pain pathway in patients with fibromyalgia: a water PET and EEG imaging study. BMC Neurology, 2018, 18, 191.	1.8	13
101	Acute Ketamine Infusion in Rat Does Not Affect In Vivo [¹¹ C]ABP688 Binding to Metabotropic Glutamate Receptor Subtype 5. Molecular Imaging, 2018, 17, 153601211878863.	1.4	13
102	Removal of the ballistocardiographic artifact from EEG–fMRI data: a canonical correlation approach. Physics in Medicine and Biology, 2009, 54, 1673-1689.	3.0	12
103	Design of a high resolution scintillator based SPECT detector (SPECTatress). Nuclear Instruments and Methods in Physics Research, Section A: Accelerators, Spectrometers, Detectors and Associated Equipment, 2011, 648, S107-S110.	1.6	12
104	The [¹⁸ F]FDG <i>μ</i> PET Readout of a Brain Activation Model to Evaluate the Metabotropic Glutamate Receptor 2 Positive Allosteric Modulator JNJ-42153605. Journal of Pharmacology and Experimental Therapeutics, 2014, 350, 375-386.	2.5	12
105	Deep Brain Stimulation of the Prelimbic Medial Prefrontal Cortex: Quantification of the Effect on Glucose Metabolism in the Rat Brain Using [18 F]FDG MicroPET. Molecular Imaging and Biology, 2014, 16, 838-845.	2.6	12
106	Synthesis and preclinical evaluation of an 18 F labeled PDE7 inhibitor for PET neuroimaging. Nuclear Medicine and Biology, 2015, 42, 975-981.	0.6	12
107	Preclinical Evaluation of a Novel ¹⁸ F-Labeled dTCO-Amide Derivative for Bioorthogonal Pretargeted Positron Emission Tomography Imaging. ACS Omega, 2020, 5, 4449-4456.	3.5	12
108	Sapap3 deletion causes dynamic synaptic density abnormalities: a longitudinal [11C]UCB-J PET study in a model of obsessive–compulsive disorder-like behaviour. EJNMMI Research, 2020, 10, 140.	2.5	12

#	Article	IF	CITATIONS
109	Effect of cyclosporin A administration on the biodistribution and multipinhole μSPECT imaging of [1231]R91150 in rodent brain. European Journal of Nuclear Medicine and Molecular Imaging, 2009, 36, 446-453.	6.4	11
110	[18F]-FDG PET neuroimaging in rats with quinpirole-induced checking behavior as a model for obsessive compulsive disorder. Psychiatry Research - Neuroimaging, 2016, 257, 31-38.	1.8	11
111	Coadministration of a Gloriosa superba extract improves the in vivo antitumoural activity of gemcitabine in a murine pancreatic tumour model. Phytomedicine, 2016, 23, 1434-1440.	5.3	11
112	Preclinical evaluation of [¹¹¹ In]MICAâ€401, an activityâ€based probe for SPECT imaging of <i>in vivo</i> uPA activity. Contrast Media and Molecular Imaging, 2016, 11, 448-458.	0.8	11
113	Baseline [18F]FMISO μPET as a Predictive Biomarker for Response to HIF-1α Inhibition Combined with 5-FU Chemotherapy in a Human Colorectal Cancer Xenograft Model. Molecular Imaging and Biology, 2016, 18, 606-616.	2.6	11
114	Markerless rat head motion tracking using structured light for brain PET imaging of unrestrained awake small animals. Physics in Medicine and Biology, 2017, 62, 1744-1758.	3.0	11
115	[99m Tc]duramycin for cell death imaging: Impact of kit formulation, purification and species difference. Nuclear Medicine and Biology, 2018, 56, 1-9.	0.6	11
116	Effects of metformin on tumor hypoxia and radiotherapy efficacy: a [18F]HX4 PET imaging study in colorectal cancer xenografts. EJNMMI Research, 2019, 9, 74.	2.5	11
117	Translation of Preclinical PET Imaging Findings: Challenges and Motion Correction to Overcome the Confounding Effect of Anesthetics. Frontiers in Medicine, 2021, 8, 753977.	2.6	11
118	GATE: Improving the computational efficiency. Nuclear Instruments and Methods in Physics Research, Section A: Accelerators, Spectrometers, Detectors and Associated Equipment, 2006, 569, 341-345.	1.6	10
119	Neural Substrates of Conversion Deafness in a Cochlear Implant Patient. Otology and Neurotology, 2014, 35, 1780-1784.	1.3	10
120	Use of a Ray-Based Reconstruction Algorithm to Accurately Quantify Preclinical MicroSPECT Images. Molecular Imaging, 2014, 13, 7290.2014.00007.	1.4	10
121	Absence of Cardiovascular Manifestations in a Haploinsufficient Tgfbr1 Mouse Model. PLoS ONE, 2014, 9, e89749.	2.5	9
122	TSPO PET upregulation predicts epileptic phenotype at disease onset independently from chronic TSPO expression in a rat model of temporal lobe epilepsy. NeuroImage: Clinical, 2021, 31, 102701.	2.7	9
123	The geometric transfer function for a slat collimator mounted on a strip detector. IEEE Transactions on Nuclear Science, 2005, 52, 708-713.	2.0	8
124	In vivo evaluation of [123I]-4-(2-(bis(4-fluorophenyl)methoxy)ethyl)-1-(4-iodobenzyl)piperidine, an iodinated SPECT tracer for imaging the P-gp transporter. Nuclear Medicine and Biology, 2010, 37, 469-477.	0.6	8
125	Low-Dose Micro-CT Imaging for Vascular Segmentation and Analysis Using Sparse-View Acquisitions. PLoS ONE, 2013, 8, e68449.	2.5	8
126	Preclinical Comparison of the Amyloid-β Radioligands [11C]Pittsburgh compound B and [18F]florbetaben in Aged APPPS1-21 and BRI1-42 Mouse Models of Cerebral Amyloidosis. Molecular Imaging and Biology, 2015, 17, 688-696.	2.6	8

#	Article	IF	CITATIONS
127	Evaluation of [¹⁸ F]BR420 and [¹⁸ F]BR351 as radiotracers for MMPâ€9 imaging in colorectal cancer. Journal of Labelled Compounds and Radiopharmaceuticals, 2017, 60, 69-79.	1.0	8
128	Elevated Type 1 Metabotropic Glutamate Receptor Availability in a Mouse Model of Huntington's Disease: a Longitudinal PET Study. Molecular Neurobiology, 2020, 57, 2038-2047.	4.0	8
129	Progression of obsessive compulsive disorder-like grooming in Sapap3 knockout mice: A longitudinal [11C]ABP688 PET study. Neuropharmacology, 2020, 177, 108160.	4.1	8
130	Motion Dependent and Spatially Variant Resolution Modeling for PET Rigid Motion Correction. IEEE Transactions on Medical Imaging, 2020, 39, 2518-2530.	8.9	8
131	Longitudinal preclinical evaluation of the novel radioligand [11C]CHDI-626 for PET imaging of mutant huntingtin aggregates in Huntington's disease. European Journal of Nuclear Medicine and Molecular Imaging, 2022, 49, 1166-1175.	6.4	8
132	Validation, kinetic modeling, and test-retest reproducibility of [¹⁸ F]SynVesT-1 for PET imaging of synaptic vesicle glycoprotein 2A in mice. Journal of Cerebral Blood Flow and Metabolism, 2022, 42, 1867-1878.	4.3	8
133	Optimization of temporal basis functions in dynamic PET imaging. Nuclear Instruments and Methods in Physics Research, Section A: Accelerators, Spectrometers, Detectors and Associated Equipment, 2006, 569, 425-428.	1.6	7
134	Automated identification of ERP peaks through Dynamic Time Warping: An application to developmental dyslexia. Clinical Neurophysiology, 2009, 120, 1819-1827.	1.5	7
135	Characterization of the ringing artifacts in rotatorâ€based reconstruction with Monte Carloâ€based resolution compensation for PET. Medical Physics, 2010, 37, 4648-4660.	3.0	7
136	In Vivo Preclinical Molecular Imaging of Repeated Exposure to an <i>N</i> -methyl-d-aspartate Antagonist and a Glutaminase Inhibitor as Potential Glutamatergic Modulators. Journal of Pharmacology and Experimental Therapeutics, 2019, 368, 382-390.	2.5	7
137	Fast 3D iterative image reconstruction for SPECT with rotating slat collimators. Physics in Medicine and Biology, 2009, 54, 715-729.	3.0	6
138	Measurement of porto-systemic shunting in mice by novel three-dimensional micro-single photon emission computed tomography imaging enabling longitudinal follow-up. Liver International, 2010, 30, 1211-1220.	3.9	6
139	Subspace electrode selection methodology for the reduction of the effect of uncertain conductivity values in the EEG dipole localization: a simulation study using a patient-specific head model. Physics in Medicine and Biology, 2012, 57, 1963-1986.	3.0	6
140	Iterative CT reconstruction using shearlet-based regularization. , 2012, , .		6
141	Continuous Flushing of the Bladder in Rodents Reduces Artifacts and Improves Quantification in Molecular Imaging, 2014, 13, 7290.2014.00013.	1.4	6
142	Prelimbic Cortical Injections of a GABA Agonist and Antagonist: In Vivo Quantification of the Effect in the Rat Brain Using [18F] FDG MicroPET. Molecular Imaging and Biology, 2015, 17, 856-864.	2.6	6
143	Characterization of an Orthotopic Colorectal Cancer Mouse Model and Its Feasibility for Accurate Quantification in Positron Emission Tomography. Molecular Imaging and Biology, 2017, 19, 762-771.	2.6	6
144	How to Modulate Tumor Hypoxia for Preclinical In Vivo Imaging Research. Contrast Media and Molecular Imaging, 2018, 2018, 1-17.	0.8	6

#	Article	IF	CITATIONS
145	Neural Substrates of Tinnitus in an Auditory Brainstem Implant Patient: A Preliminary Molecular Imaging Study Using H2 15 O-PET Including a 5-year Follow-up of Auditory Performance and Tinnitus Perception. Otology and Neurotology, 2020, 41, e15-e20.	1.3	6
146	[¹⁸ F]ZCDD083: A PFKFB3-Targeted PET Tracer for Atherosclerotic Plaque Imaging. ACS Medicinal Chemistry Letters, 2020, 11, 933-939.	2.8	6
147	Decreased levels of active <scp>uPA</scp> and <scp>KLK</scp> 8 assessed by [¹¹¹ In] <scp>MICA</scp> â€401 binding correlate with the seizure burden in an animal model of temporal lobe epilepsy. Epilepsia, 2017, 58, 1615-1625.	5.1	5
148	Kinetic Modelling and Test–Retest Reproducibility for the Dopamine D1R Radioligand [11C]SCH23390 in Healthy and Diseased Mice. Molecular Imaging and Biology, 2021, 23, 208-219.	2.6	5
149	Degradation of myocardial perfusion SPECT images caused by contaminants in thallous (201Tl) chloride. European Journal of Nuclear Medicine and Molecular Imaging, 2008, 35, 922-932.	6.4	4
150	Monte Carlo Simulations in Nuclear Medicine Imaging. , 2009, , 177-209.		4
151	Longitudinal follow-up of ascending versus abdominal aortic aneurysm formation in angiotensin II-infused ApoEâ^'/â^' mice. Artery Research, 2014, 8, 16.	0.6	4
152	Clutaminase activity in GLS1 Het mouse brain compared to putative pharmacological inhibition by ebselen using ex vivo MRS. Neurochemistry International, 2019, 129, 104508.	3.8	4
153	FIRST RESULTS WITH THE CLEARPET SMALL ANIMAL PET SCANNERS. , 2006, , 149-164.		4
154	Sensitivity of SPECT with rotating slat collimators. , 0, , .		3
155	The Heterozygous Lemd3 +/GT Mouse Is Not a Murine Model for Osteopoikilosis in Humans. Calcified Tissue International, 2009, 85, 546-551.	3.1	3
156	Tomographic image quality of rotating slat versus parallel hole-collimated SPECT. Physics in Medicine and Biology, 2011, 56, 7205-7222.	3.0	3
157	O2-07-05: Investigations of brain glucose utilization in three transgenic mouse strains that develop neuropathological features of Alzheimer's disease. , 2013, 9, P329-P329.		3
158	In Vivo Amyloid-β Imaging in the APPPS1–21 Transgenic Mouse Model with a 89Zr-Labeled Monoclonal Antibody. Frontiers in Aging Neuroscience, 2016, 8, 67.	3.4	3
159	Early Changes in [18F]FDG Uptake as a Readout for PI3K/Akt/mTOR Targeted Drugs in HER-2-Positive Cancer Xenografts. Molecular Imaging, 2021, 2021, 1-14.	1.4	3
160	Simulation study comparing the imaging performance of a solid state detector with a rotating slat collimator versus parallel beam collimator setups. , 2004, , .		2
161	Transmission imaging with a moving point source: influence of crystal thickness and collimator type. IEEE Transactions on Nuclear Science, 2005, 52, 166-173.	2.0	2
162	PET Reconstruction Using Generalized Natural Pixels and a Monte Carlo Generated System Matrix. , 2006, , .		2

#	Article	IF	CITATIONS
163	Comparison of 3D SPECT imaging with a rotating slat collimator and a parallel hole collimator. , 2008, , .		2
164	Fan beam forced detection in Gate. , 2009, , .		2
165	Simulation of complex geometries in GATE. , 2009, , .		2
166	A high resolution scintillator based SPECT detector with digital pulse processing (SPECTatress). , 2010, , .		2
167	Influence of skull inhomogeneities on EEG source localization. , 2011, , .		2
168	Evaluation of [18F]Fluorothymidine as a Biomarker for Early Therapy Response in a Mouse Model of Colorectal Cancer. Molecular Imaging and Biology, 2017, 19, 109-119.	2.6	2
169	Neuroreceptor kinetics in rats repeatedly exposed to quinpirole as a model for OCD. PLoS ONE, 2019, 14, e0213313.	2.5	2
170	Low activity [11C]raclopride kinetic modeling in the mouse brain using the spatiotemporal kernel method. Physics in Medicine and Biology, 2021, 66, 115005.	3.0	2
171	Estimation of the net influx rate Ki and the cerebral metabolic rate of glucose MRglc using a single static [18F]FDG PET scan in rats. NeuroImage, 2021, 233, 117961.	4.2	2
172	Compression and reconstruction of sorted PET listmode data. Nuclear Medicine Communications, 2005, 26, 819-825.	1.1	1
173	A penalized Algebraic Reconstruction Technique (pART) for PET image reconstruction. , 2007, , .		1
174	Contrast noise behaviour of a rotating slat collimated gamma camera. Nuclear Instruments and Methods in Physics Research, Section A: Accelerators, Spectrometers, Detectors and Associated Equipment, 2007, 571, 274-277.	1.6	1
175	Monte-Carlo system modeling for PET reconstruction: A rotator approach. , 2008, , .		1
176	Using GATE as a forward projector in iterative SPECT reconstruction. , 2008, , .		1
177	Scatter effects of MR components in PET-MR inserts. , 2009, , .		1
178	Effect of geometrical constraints on PET performance in whole body simultaneous PET-MR. , 2009, , .		1
179	IC-P-044: LONGITUDINAL MONITORING OF Î ² -AMYLOID PATHOLOGY AND CEREBRAL HYPOMETABOLISM IN A DOUBLE TRANSGENIC MOUSE MODEL OF ALZHEIMER'S DISEASE. , 2014, 10, P27-P27.		1
180	MicroPET Outperforms Beta-Microprobes in Determining Neuroreceptor Availability under Pharmacological Restriction for Cold Mass Occupancy. Frontiers in Neuroscience, 2017, 11, 47.	2.8	1

#	Article	IF	CITATIONS
181	Spatially variant point spread function for PET rigid motion correction. , 2019, , .		1
182	Molecular Imaging of mGluR5 Availability with [11C]ABP68 in Glutaminase Heterozygous Mice. Cellular and Molecular Neurobiology, 2019, 39, 255-263.	3.3	1
183	Quantification of Metabotropic Glutamate Receptor 5 Availability With Both [11C]ABP688Âand [18F]FPEB Positron Emission Tomography in the Sapap3 Knockout Mouse Model for Obsessive-Compulsive–like Behavior. Biological Psychiatry: Cognitive Neuroscience and Neuroimaging, 2022, 7, 607-615.	1.5	1
184	Correction for partial volume effects in brain perfusion ECT imaging. , 2003, , .		0
185	Theoretical LOR model incorporating spatial uncertainty in continuous detector PET. , 2003, , .		Ο
186	Transmission imaging with a moving point source: influence of crystal thickness and collimator type. , 0, , .		0
187	Analytical model for Solstice detector response. , 0, , .		Ο
188	Optimizing the Scalability of Parallelized GATE Simulations. , 2006, , .		0
189	LROC assessment of non-linear filtering methods in Ga-67 SPECT imaging. , 2006, 6146, 106.		Ο
190	Acceleration of GATE SPECT simulations. , 2007, , .		0
191	High resolution μSPECT for brain activation analysis in small animals. , 2009, , .		Ο
192	Epileptogenic focus localization through connectivity analysis of the intracranial EEG: A retrospective study in 2 patients. , 2011 , , .		0
193	A20 (TNFAIP3) deficiency in myeloid cells triggers rheumatoid arthritis. Annals of the Rheumatic Diseases, 2011, 70, A39-A40.	0.9	0
194	Su1934 Activation Status of the Central Nervous System and Lumbar Dorsal Root Ganglia in a Mouse Model of Polymicrobial Abdominal Septic Ileus. Gastroenterology, 2016, 150, S592-S593.	1.3	0
195	Abstract 3910: Targeting urokinase plasminogen activator: evaluation of activity-based imaging probes in an orthotopic breast cancer model , 2013, , .		0
196	Small Animal Molecular Imaging Through μPET and μSPECT. , 2014, , 47-84.		0
197	Abstract 1875: [18F]HX4 shows potential as a predictive biomarker for the radiosensitizing capacities of metformin in a NSCLC xenograft model. , 2017, , .		0
198	Spatiotemporal Kernel Reconstruction for Linear Parametric Neurotransmitter PET Kinetic Modeling in Motion Correction Brain PET of Awake Rats. Frontiers in Neuroscience, 2022, 16, .	2.8	0